Chapter 12
Is Load Application Necessary when Using Computed Tomography Scans to Diagnose Syndesmotic Injuries? A Cadaver Study

Alexej Barg

Introduction

Injury to the distal tibiofibular syndesmosis is common and appears in up to 20% of patients with an ankle sprain or ankle fracture [1–3]. If not treated appropriately, long-lasting disabilities like chronic pain, instability, and ankle joint osteoarthritis may occur [2, 4, 5]. Injury can occur to any of the four main components of the distal tibiofibular syndesmosis: the anterior inferior tibiofibular ligament (AITFL), interosseous membrane (IOM), posterior inferior tibiofibular ligament (PITFL), and transverse tibiofibular ligament (TTFL) [2, 3, 6]. Additionally, a deltoid ligament injury is also frequently present in patients with syndesmotic injury [7].

Conventional (weight-bearing) radiographs (anteroposterior and mortise view) (Fig. 12.1), CT scans (Fig. 12.2), and magnetic resonance imaging (MRI) (Fig. 12.3) are widely used for assessment of the distal tibiofibular syndesmosis [3].

While pronounced injuries can be reliably assessed using conventional radiographs, the diagnosis of incomplete injuries, especially in the absence of a fracture (e.g., high ankle sprain), is difficult [8–11]. In addition, measurements on conventional radiographs do not reliably reflect the injury pattern, which limits the general utility of conventional radiographs in assessing the distal tibiofibular syndesmosis [12]. Correlating findings in magnetic resonance imaging (MRI) with patient complaints can prove challenging [3]. Therefore, an accurate imaging modality to assess patients with incomplete injuries to the distal tibiofibular syndesmosis is desirable.

With the introduction of weight-bearing CT scans, detailed assessment of foot and ankle disorders under load-bearing conditions became possible [13–15].

Tibiofibular Clear Space	Superior Clear Space	Talocrural Angle	Tibiofibular Overlap	Medial Clear Space	Height of Incisura
X-ray	X-ray	X-ray	X-ray	X-ray	X-ray / 3-D
Coronal (AP)	Coronal (AP)	Mortise View	Mortise View	Mortise View	Coronal (AP)
Axial	Sagittal	Mortise View (detail)	Axial	Axial	Sagittal (3D reconstruction)

Fig. 12.1 Frequently used measurement methods to assess the distal tibiofibular syndesmosis using plain radiographs [3]

However, the impact of load on two-dimensional (2D) measurements performed on axial CT images to assess the integrity of the distal tibiofibular syndesmosis is debated [16, 17]. The purpose of this cadaver study was to assess the influence of weight on the assessment of incomplete and more complete syndesmotic injuries using 2D measurements on axial CT images. We hypothesized that weight would significantly impact on the assessment of both incomplete and more complete injuries to the distal tibiofibular syndesmosis.

Methods

Data Source

Seven pairs of male cadavers (tibia plateau to toe-tip) were included (mean age 62 ± 7 [range 52–70] years; mean weight 84.9 ± 15.3 [range 65.8–104.8] kg; mean body mass index (BMI) 26.8 ± 5.0 [range 19.7–32.5] kg/m^2). Inclusion criteria were 20–70 years of age and a BMI of less than 35 kg/m^2. Exclusion criteria were a history of any foot and ankle injuries or a history of surgery of the foot and ankle.
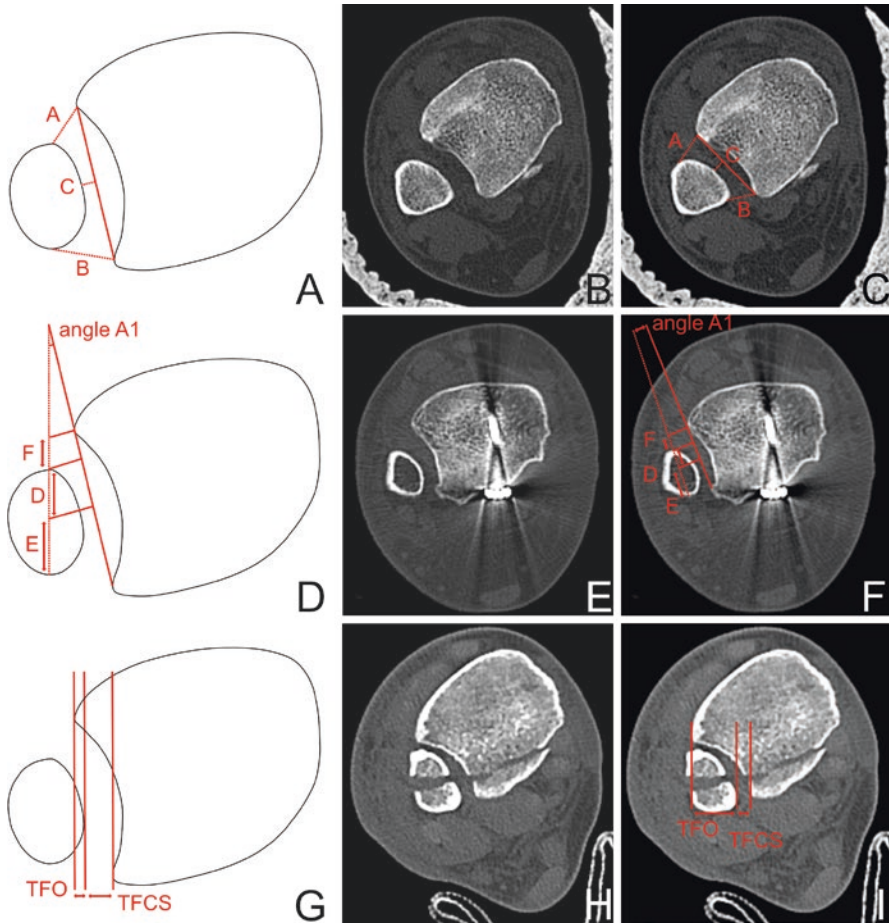
Fig. 12.2 Frequently used measurement methods to assess the distal tibiofibular syndesmosis using computed tomography (CT) scans. Measurements were performed 1 cm above the distal tibial plafond. (**a**) Measurement of the tibiofibular width anterior (**a**), middle (**c**), and posterior (**b**). (**b**) A 35-year-old patient with an acute syndesmotic instability following a high fibular and posterior malleolar fracture. The syndesmotic injury was not addressed on the primary surgery. (**c**) Measurement of the tibiofibular width. (**d**) Measurement of the anteroposterior translation (**d**–**f**) and the rotation (angle A1) of the distal fibula. (**e**) A 47-year-old patient with an acute syndesmotic injury following a high fibular fracture and small posterior malleolar avulsion. (**f**) Measurement of the anteroposterior translation and rotation of the distal fibula. (**g**) Measurement of the tibiofibular clear space (TFCS) and tibiofibular overlap (TFO). (**h**) A 37-year-old patient with an acute syndesmotic injury following a high fibular fracture. (**i**) Measurement of the TFCS and TFO. Radiologists and orthopedic surgeons should be aware that a distal fracture of the fibula and/or an additional tibia fracture influence the measurements. It is important to mention that the rotation of the ankle also influences the measurements [3]
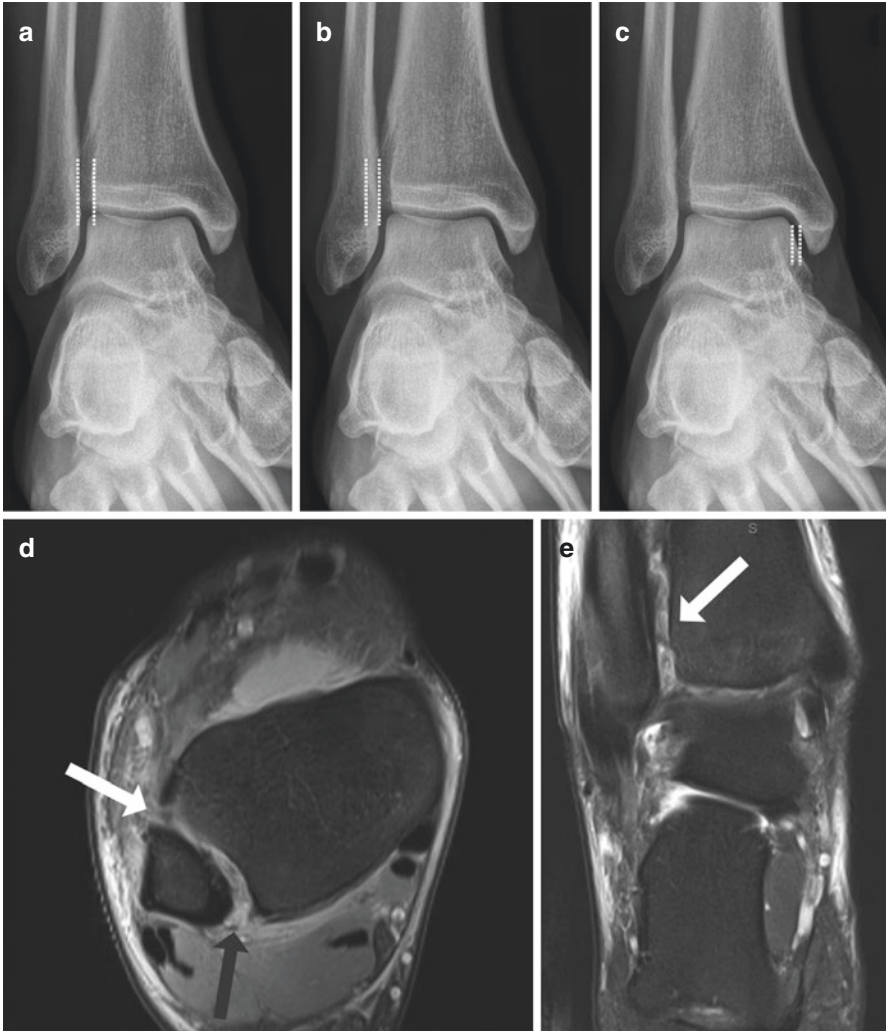
Fig. 12.3 Example of a 37-year-old man with an acute isolated syndesmotic injury. The conventional radiographs (mortise view) cannot predict reliably the syndesmotic injury. (**a**) Normal tibiofibular clear space (TFCS). (**b**) Normal tibiofibular overlap (TFO). (**c**) Normal medial clear space (MCS). (**d**) Axial magnet resonance imaging (MRI) proton density with fat saturation demonstrates full-thickness tear of both the anterior (white arrow) and posterior (grey arrow) tibiofibular ligaments. (**e**) Coronal T2 fat-saturated MRI image shows heterogeneity and increased signal of the syndesmotic ligaments (arrow), consistent with syndesmotic injury [3]

Experimental Setting

Each specimen was thawed for 24 hours at room temperature before any experiments were performed [18]. A radiolucent frame held the specimens in a plantigrade position (Fig. 12.4). The cadaver was fixed with an Ilizarov apparatus that fit into the frame. Four 1.5 mm Kirschner-wires (K-wires) were drilled through the tibia for fixation to the frame. The K-wires were tightened using a dynamometric wire tensioner (Smith & Nephew). The hindfoot was fixed using two 1.5 mm K-wires drilled through the calcaneus, and two-part resin (Bondo®, 3 M) stabilized the soft tissue envelope below the level of the syndesmotic ligaments. Non-weight-bearing and weight-bearing CT scans were collected (PedCAT, CurveBeam LLC, Warrington, USA, medium view, 0.3 mm slice thickness, 0.3 mm slice interval, kVp 120, mAs 22.62).

First, intact ankles (native) were scanned. Second, one specimen from each pair underwent AITFL transection (Condition 1A), while the contralateral underwent deltoid transection (Condition 1B). Third, the lesions were reversed on the same specimens, and the remaining intact deltoid ligament or AITFL was transected in each ankle (Condition 2). Finally, the interosseous membrane (IOM) was transected

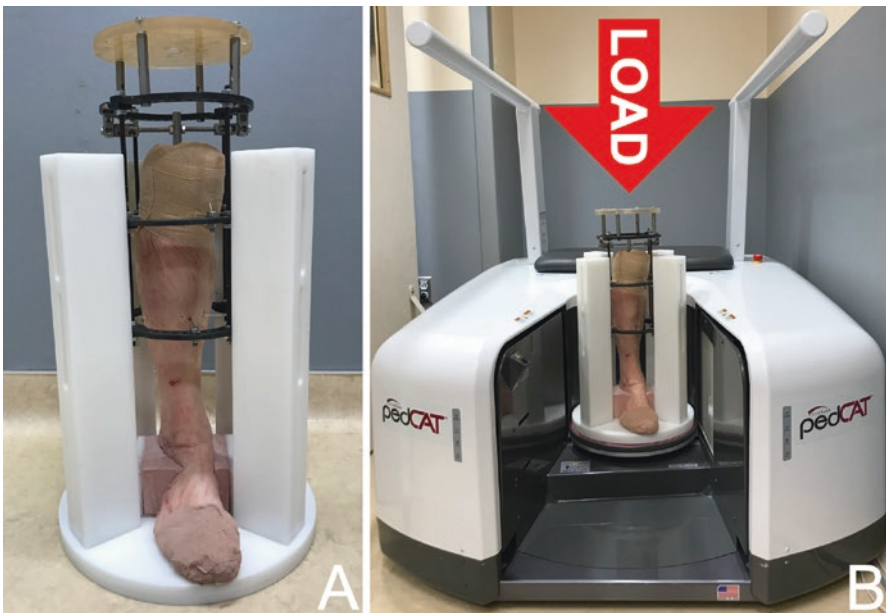**Fig. 12.4** Experimental setting. (**a**) The foot was fixed in an Ilizarov frame, which fit into a radiolucent frame that held the foot in a plantigrade position. The hindfoot was fixed with two Kirschner-wires (K-wires) and a two-part resin (Bondo®, 3 M). (**b**) The frame was put into a weight-bearing computed tomography (CT) scanner for data collection. Load was applied to the plate mounted on top of the Ilizarov frame [1]

in all ankles (Condition 3). Conditions 1A and 1B were considered to mimic incomplete injuries, while Conditions 2 and 3 were considered to mimic more complete injuries. For each condition, non-weight-bearing, half-bodyweight (42.5 kg), and full-bodyweight (85 kg) CT scans were taken. Loading levels were determined from the average of specimen donor anthropometrics. Preconditioning of the specimen was performed by statically loading the frame with 42.5 kg and 85 kg for 2 minutes each before the experiments were performed.

Measurements for interobserver agreement calculation were done by a fellowship-trained orthopedic surgeon and a research analyst. For calculation of the intraobserver agreement, measurements were performed two times with an interval of 3 weeks by a fellowship-trained orthopedic surgeon. Each observer completed a computer-based training before measurements were performed.

Imaging and Measurements

Axial CT images 1 cm above the medial edge of the distal tibial plafond were reconstructed (CurveBeam LLC, Warrington, USA, Version 3.2.1.0) and used for the following measurements: distance between the most anterior point of the tibial incisura and the nearest most anterior point of the fibula (ATFD), distance between the most anterior point of the fibula and a line perpendicular to the most anterior point of the tibial incisura (AFT), distance between the most anterior point of the fibula and a line perpendicular to the connection of the most anterior and posterior point of the tibial incisura (MFT), and distance from the same perpendicular line to the most posterior point of the fibula (PFT, Fig. 12.5) [16, 17, 19]. In addition, the angle between the fibular axis (the line between the most anterior and posterior edge of the fibula) and the line between the anterior and posterior edge of the tibial incisura were measured (Angle 1) [19]. Furthermore, the tibiofibular overlap (TFO, defined as the maximum overlap between the lateral tibia and medial fibula) and the tibiofibular clear space (TFCS, defined as the distance from the lateral border of the posterior tibial tubercle to the medial border of the fibula) were measured on the same axial images [20]. On the level of the talar dome (axial images), the angle between the fibula and medial malleolus (Angle 2) was measured [19].

Statistical Analysis

Intraclass correlation (ICC) was used to quantify the agreement of measurements between and within observers. Estimates and 95% confidence intervals (CI) were calculated for each type of measurement. Interobserver agreement was modeled with a two-way random effect model of absolute agreement with a single measure-

Fig. 12.5 Measurements using computed tomography (CT) scans. (**a**) Axial image 1 cm above of the tibial plafond. The anterior tibiofibular distance (ATFD) represents the distance between the most anterior point of the tibial incisura and the most anterior point of the fibula. The anterior fibular translation (AFT) is defined as the distance between the most anterior point of the fibula and a perpendicular line to the anterior edge of the tibial incisura. The middle fibular translation (MFT) is defined as the distance between the most anterior point of the fibula and a line perpendicular to the connection of the most anterior and posterior point of the tibial incisura. The posterior fibular translation (PFT) represents the distance between the most posterior point of the fibula and the same perpendicular line. Angle 1 represents the angle between a line drawn between the most anterior and posterior point of the tibial incisura and the axis of the fibula. (**b**) Tibiofibular clear space (TFCS) and tibiofibular overlap (TFO) measured 1 cm above the tibial plafond. (**c**) Angle 2 measured between the fibula and the medial malleolus at the level of the tibial dome [1]
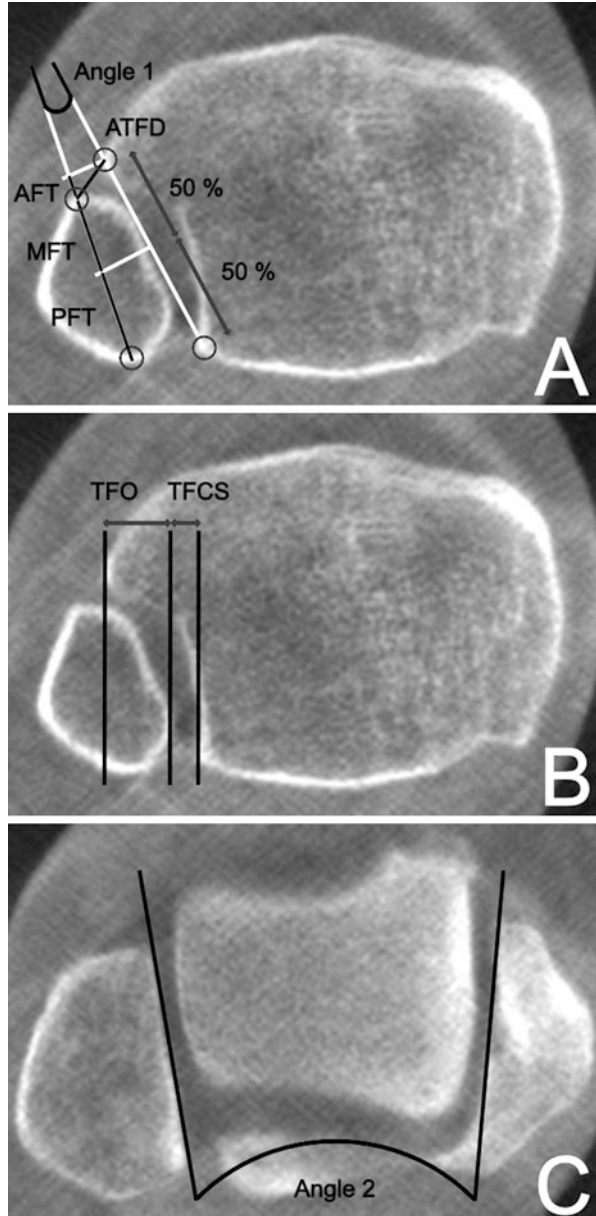
ment per observation. Intraobserver agreement was modeled with a two-way mixed effect model of consistency with a single measurement per observation. Agreement was rated as excellent with an ICC >0.75; good with an ICC = 0.61–0.75; fair with an ICC = 0.4–0.6; and poor with an ICC <0.4 [16].

Linear mixed effect models were fit for responses. Cadaver, treated as a random effect, and foot, (left or right) treated as a fixed effect, were included in all models in addition to the variables presented lateral in the tables. Models were fit for subsets of the data (with given weight or condition constant) and estimates and 95% CI are given for differing levels of condition or weight. Confidence intervals were calculated using a Tukey adjustment for multiple comparisons within each model. Significance was determined based on a P-value of less than 0.05 after the Tukey adjustment. All calculations were done in R 3.4.1, specifically using package psych and ImerTest.

Results

Inter- and intraobserver agreement differed between measurements (Table 12.1). Excellent agreement was evident for the TFCS and TFO (intraobserver agreement, 0.79 and 0.94). Poor agreement was evident for Angle 1 (interobserver, 0.39). The agreement of the other measurements (inter- and intraobserver) was either rated as fair or good and ranged from 0.44 to 0.71. Load application had no significant influence on almost every measurement across all conditions (e.g., without subdividing into different conditions; Table 12.2). Divided into the tested conditions, only the ATFD or TFO could identify more complete injuries (Condition 3) from native ankles (Tables 12.3 and 12.4). No significant differences were evident between single AITFL and deltoid ligament transection for the ATFD and TFO. No significant differences were observed within each condition between non-, half-, and full-weight-bearing when using the ATFD or TFO (Tables 12.5 and 12.6).

Table 12.1 Agreement of computed tomography scans assessed by intraclass correlation (ICC) [1]

	Interobserver: ICC(2,1) *Estimate (95% CI)*	Level of agreement	Intraobserver: ICC(3,1) *Estimate (95% CI)*	Level of agreement
Angle 1	0.39 (0.12, 0.60)	Poor	0.51 (0.27, 0.69)	Fair
Angle 2	0.44 (−0.08, 0.74)	Fair	0.67 (0.48, 0.80)	Good
ATFD	0.54 (0.30, 0.71)	Fair	0.58 (0.35, 0.74)	Fair
AFT	0.65 (0.45, 0.79)	Good	0.61∗ (0.39, 0.76)	Good
MFT	0.65 (0.45, 0.79)	Good	0.71∗ (0.53, 0.82)	Good
PFT	0.53 (0.29, 0.70)	Fair	0.54 (0.30, 0.71)	Fair
TFCS	0.61 (0.74, 0.97)	Good	0.79 (0.89, 0.97)	Excellent
TFO	0.57 (0.53, 0.98)	Fair	0.94 (0.97, 0.99)	Excellent

CT computed tomography, *CI* confidence interval, *ATFD* anterior tibiofibular distance, *AFT* anterior fibular translation, *MFT* middle fibular translation, *PFT* posterior fibular translation, *TFCS* tibiofibular clear space, *TFO* tibiofibular overlap
∗Significant difference (*P*-value <0.05)

Table 12.2 Influence of load on computed tomography measurements across all tested conditions (difference between weight application in millimeters [mm]) [1]

		Mean (SD; mm)	Estimate (95% CI)	
			Non-weight-bearing	Half-bodyweight
Angle 1	Non-weight-bearing	−13.3 (5.8)	–	–
	Half-bodyweight	−13.4 (5.3)	0.0 (−1.8, 1.8)	–
	Full-bodyweight	−13.8 (5.4)	−0.5 (−2.2, 1.3)	−0.4 (−2.2, 1.4)
Angle 2	Non-weight-bearing	10.3 (7.5)	–	–
	Half-bodyweight	10.8 (7.9)	0.5 (−0.8, 1.8)	–
	Full-bodyweight	11.1 (7.4)	0.8 (−0.5, 2.1)	0.3 (−1.0, 1.6)
ATFD	Non-weight-bearing	4.6 (1.0)	–	–
	Half-bodyweight	4.7 (1.3)	0.1 (−0.4, 0.5)	–
	Full-bodyweight	4.5 (1.0)	−0.1 (−0.5, 0.3)	−0.2 (−0.6, 0.3)
AFT	Non-weight-bearing	2.3 (1.6)	–	–
	Half-bodyweight	2.1 (1.5)	−0.1 (−0.6, 0.3)	–
	Full-bodyweight	1.0 (1.5)	−0.3 (−0.7, 0.2)	−0.2 (−0.6, 0.3)
MFT	Non-weight-bearing	9.3 (1.5)	–	–
	Half-bodyweight	9.4 (1.4)	0.1 (−0.3, 0.6)	–
	Full-bodyweight	9.7 (1.4)	0.4 (−0.1, 0.8)	0.3 (−0.2, 0.7)
PFT	Non-Weight-bearing	8.1 (1.2)	–	–
	Half-bodyweight	7.9 (1.1)	−0.1 (−0.5, 0.3)	–
	Full-bodyweight	7.6 (1.1)	**−0.4∗ (0.8, −0.0)**	−0.3 (−0.7, 0.1)
TFCS	Non-Weight-bearing	4.5 (1.6)	–	–
	Half-bodyweight	4.7 (1.5)	0.2 (−0.2, 0.5)	–
	Full-bodyweight	4.7 (1.5)	0.1 (−0.3, 0.5)	−0.1 (−0.4, 0.3)
TFO	Non-Weight-bearing	6.2 (1.5)	–	–
	Half-bodyweight	6.1 (1.5)	−0.1 (−0.7, 0.4)	–
	Full-bodyweight	6.2 (1.4)	0.0 (−0.5, 0.5)	0.1 (−0.4, 0.7)

SD standard deviation, *CT* computed tomography, *CI* confidence interval, *ATFD* anterior tibiofibular distance, *AFT* anterior fibular translation, *MFT* middle fibular translation, *PFT* posterior fibular translation, *TFCS* tibiofibular clear space, *TFO* tibiofibular overlap
∗Significant difference (*P*-value <0.05)

Discussion

A cadaver study testing the impact of weight on assessment of syndesmotic injuries using axial CT images was performed. The three most relevant findings were the following: (1) weight did not improve the ability of most 2D measurements to diagnose syndesmotic injuries; (2) only more complete injuries could be identified using weight-bearing CT scans; and (3) discrete AITFL and deltoid ligament injuries could not be distinguished.

Multiple studies investigating the utility of weight-bearing radiographs or non-weight-bearing CT scans in the diagnoses of injuries to the distal tibiofibular syndesmosis have been published [8–10, 12, 21, 22]. In contrast, only two studies assessed the impact of load on the assessment of the distal tibiofibular syndesmosis

Table 12.3 Influence of ligament resection on anterior tibiofibular distance (computed tomography; difference between each condition in millimeters [mm]) [1]

ATFD		Mean (SD; mm)	Estimate (95% CI) Native	Condition 1A	Condition 1B	Condition 2
Non-weight-bearing	Native	4.0 (0.9)	–	–	–	–
	Condition 1A	4.5 (0.7)	0.5 (−0.5, 1.5)	–	–	–
	Condition 1B	4.4 (0.6)	0.4 (−0.6, 1.4)	−0.1 (−1.2, 1.0)	–	–
	Condition 2	4.5 (0.9)	0.5 (−0.3, 1.3)	0.0 (−1.0, 1.0)	0.1 (−0.9, 1.1)	–
	Condition 3	5.4 (1.0)	**1.4∗ (0.6, 2.2)**	0.9 (−0.1, 1.9)	**1.0∗ (0.0, 2.0)**	**0.9∗ (0.1, 1.7)**
Half-bodyweight	Native	3.8 (1.0)	–	–	–	–
	Condition 1A	4.8 (1.2)	1.0 (−0.2, 2.2)	–	–	–
	Condition 1B	4.1 (1.0)	0.4 (−0.8, 1.5)	−0.7 (−2.0, 0.7)	–	–
	Condition 2	4.7 (0.9)	0.93 (−0.02, 1.88)	−0.1 (−1.2, 1.1)	0.6 (−0.6, 1.7)	–
	Condition 3	5.7 (1.4)	**1.9∗ (1.0, 2.9)**	0.9 (−0.3, 2.1)	**1.6∗ (0.4, 2.7)**	**1.0∗ (0.0, 1.9)**
Full-bodyweight	Native	4.0 (0.9)	–	–	–	–
	Condition 1A	4.6 (1.0)	0.5 (−0.4, 1.5)	–	–	–
	Condition 1B	3.9 (0.9)	−0.1 (−1.1, 0.8)	−0.7 (−1.7, 0.4)	–	–
	Condition 2	4.6 (0.9)	0.6 (−0.1, 1.3)	0.1 (−0.9,1.0)	0.7 (−0.2, 1.6)	–
	Condition 3	5.1 (1.0)	**1.1∗ (0.3, 1.8)**	0.5 (−0.4, 1.4)	**1.2∗ (0.3, 2.1)**	0.5 (−0.3, 1.2)

CT computed tomography, *SD* standard deviation, *CI* confidence interval, *ATFD* anterior tibiofibular distance

∗Significant difference (*P*-value <0.05)

when using CT scans [16, 17]. Shakoor et al. did not find any significant differences when load was applied for most measurements (asymptomatic ankles included), while Malhotra et al. found that the fibula rotates posterolateral under weight-bearing conditions [16, 17]. Of note, Malhotra et al. did use different CT scanners for weight-bearing and non-weight-bearing imaging [17]. Also, the included cohort was not uniform (e.g., ankles with different pathologies) [17]. This may impact on the assessment of the distal tibiofibular syndesmosis when using axial CT images as 2D measurements are dependent on the position of the ankle joint (e.g., rotation and plantar flexion/dorsal extension) [23, 24]. The present cadaver study supports the findings by Shakoor et al. and showed no differences between 2D measurements with and without load application.

Although loading may not be crucial, weight-bearing CT scans have several advantages over other imaging options: first, the position of the foot can be standardized using weight-bearing CT scans, allowing imaging with the foot in a plantigrade position in the same relative rotation to the body and/or scanner. Second, some weight-bearing CT scans also allow both feet to be scanned at the same time. As the anatomy of the tibial incisura varies between individuals, a left-right comparison can highlight certain injuries and abnormalities that would otherwise go unnoticed [25–29].

The inter- and intraobserver agreement between measurements differed in the present study. Defining anatomical landmarks on axial CT images can be difficult.

Table 12.4 Influence of ligament resection on tibiofibular overlap measurements (computed tomography; difference between each condition in millimeters [mm]) [1]

TFO		Mean (SD; mm)	Estimate (95% CI)			
			Native	Condition 1A	Condition 1B	Condition 2
Non-weight-bearing	Native	6.8 (1.6)	–	–	–	–
	Condition 1A	5.9 (1.2)	−0.9 (−2.4, 0.6)	–	–	–
	Condition 1B	6.7 (1.4)	−0.1 (−1.6, 1.4)	0.8 (−1.0, 2.6)	–	–
	Condition 2	6.3 (1.7)	−0.5 (−1.8, 0.7)	0.4 (−1.2, 1.9)	−0.4 (−1.9, 1.1)	–
	Condition 3	5.5 (1.3)	**−1.3*** **(−2.5, −0.0)**	−0.4 (−1.9, 1.2)	−1.2 (−2.7, 0.4)	−0.7 (−2.0, 0.5)
Half-bodyweight	Native	6.7 (1.6)	–	–	–	–
	Condition 1A	6.0 (1.6)	−0.7 (−2.0, 0.7)	–	–	–
	Condition 1B	6.6 (1.2)	−0.1 (−1.5, 1.2)	0.5 (−1.0, 2.1)	–	–
	Condition 2	6.0 (1.5)	−0.7 (−1.8, 0.4)	−0.1 (−1.4, 1.3)	−0.6 (−1.0, 0.8)	–
	Condition 3	5.4 (1.9)	**−1.3*** **(−2.4, −0.2)**	−0.6 (−1.0, 0.7)	−1.2 (−2.5, 0.2)	−0.6 (−1.7, 0.6)
Full-bodyweight	Native	6.9 (1.5)	–	–	–	–
	Condition 1A	6.1 (1.0)	−0.8 (−2.2, 0.6)	–	–	–
	Condition 1B	6.9 (1.4)	−0.0 (−1.4, 1.4)	0.8 (−0.8, 2.4)	–	–
	Condition 2	6.0 (1.1)	−0.9 (−2.1, 0.2)	−0.09 (−1.5, 1.3)	−0.9 (−2.3, 0.5)	–
	Condition 3	5.4 (1.3)	**−1.5*** **(−2.6, −0.4)**	−0.7 (−2.1, 0.7)	**−1.5*** **(−2.9, −0.1)**	−0.6 (−1.7, 0.6)

CT computed tomography, *SD* standard deviation, *CI* confidence interval, *TFO* tibiofibular overlap
*Significant difference (P-value <0.05)

The anatomy of the fibula and the incisura of the tibia differ between individuals, and edges can either be round or sharp (Fig. 12.6) [22, 25–28]. This may be the reason why Angle 1 and Angle 2 showed the lowest agreement compared to the other measurements: four anatomic landmarks had to be defined for each of these two measurements while most other measurement only required two. Also, interobserver agreement was lower compared to intraobserver agreement for every measurement. As measurements were performed by a fellowship orthopedic surgeon and a research analyst less experienced in imaging analysis, our results suggest that the agreement of 2D measurements are dependent on the experience of the observer.

Table 12.5 Influence of weight on anterior tibiofibular distance (computed tomography; difference between weight application in millimeters [mm]) [1]

ATFD		Mean (SD; mm)	Estimate (95% CI) Non-weight-bearing	Half-bodyweight
Native	Non-weight-bearing	4.0 (0.9)	–	–
	Half-bodyweight	3.8 (1.0)	−0.3 (−0.8, 0.3)	–
	Full-bodyweight	4.0 (0.9)	0.0 (−0.5, 0.5)	0.3 (−0.3, 0.8)
Condition 1A	Non-weight-bearing	4.5 (0.8)	–	–
	Half-bodyweight	4.8 (1.2)	0.3 (−0.3, 0.9)	–
	Full-bodyweight	4.6 (1.0)	0.1 (−0.5, 0.7)	−0.2 (−0.8, 0.4)
Condition 1B	Non-weight-bearing	4.4 (0.6)	–	–
	Half-bodyweight	4.1 (0.9)	−0.2 (−1.0, 0.5)	–
	Full-bodyweight	3.9 (0.9)	−0.5 (−1.3, 0.3)	−0.3 (−1.0, 0.5)
Condition 2	Non-weight-bearing	4.5 (0.9)	–	–
	Half-bodyweight	4.7 (0.9)	0.2 (−0.5, 0.9)	–
	Full-bodyweight	4.6 (0.9)	0.1 (−0.6, 0.8)	−0.1 (−0.8, 0.6)
Condition 3	Non-weight-bearing	5.4 (1.0)	–	–
	Half-bodyweight	5.7 (1.4)	0.3 (−0.6, 1.2)	–
	Full-bodyweight	5.1 (1.0)	−0.3 (−1.2, 0.6)	−0.6 (−1.5, 0.3)

CT computer tomography, *SD* standard deviation, *CI* confidence interval, *ATFD* anterior tibiofibular distance
*Significant difference (*P*-value <0.05)

Table 12.6 Influence of weight on tibiofibular overlap measurements (computed tomography; difference between weight application in millimeters [mm]) [1]

TFO		Mean (SD; mm)	Estimate (95% CI) Non-weight-bearing	Half-bodyweight
Native	Non-weight-bearing	6.8 (1.6)	–	–
	Half-bodyweight	6.7 (1.6)	−0.1 (−1.2, 1.0)	–
	Full-bodyweight	6.9 (1.5)	0.1 (−1.0, 1.3)	0.2 (−0.9, 1.3)
Condition 1A	Non-weight-bearing	5.9 (1.2)	–	–
	Half-bodyweight	6.0 (1.6)	0.1 (−0.4, 0.7)	–
	Full-bodyweight	6.1 (1.0)	0.2 (−0.3, 0.7)	0.0 (−0.5, 0.6)
Condition 1B	Non-weight-bearing	6.7 (1.4)	–	–
	Half-bodyweight	6.6 (1.2)	−0.1 (−0.7, 0.4)	–
	Full-bodyweight	6.9 (1.4)	0.2 (−0.3, 0.8)	0.3 (−0.2, 0.9)
Condition 2	Non-weight-bearing	6.3 (1.7)	–	–
	Half-bodyweight	6.0 (1.5)	−0.3 (−1.2, 0.6)	–
	Full-bodyweight	6.0 (1.1)	−0.3 (−1.2, 0.6)	0.0 (−0.9, 0.9)
Condition 3	Non-weight-bearing	5.5 (1.3)	–	–
	Half-bodyweight	5.4 (1.2)	−0.1 (−1.0, 0.8)	–
	Full-bodyweight	5.4 (1.3)	−0.1 (1.0, 0.8)	0.0 (−0.9, 0.9)

CT computer tomography, *SD* standard deviation, *CI* confidence interval, *TFO* tibiofibular overlap
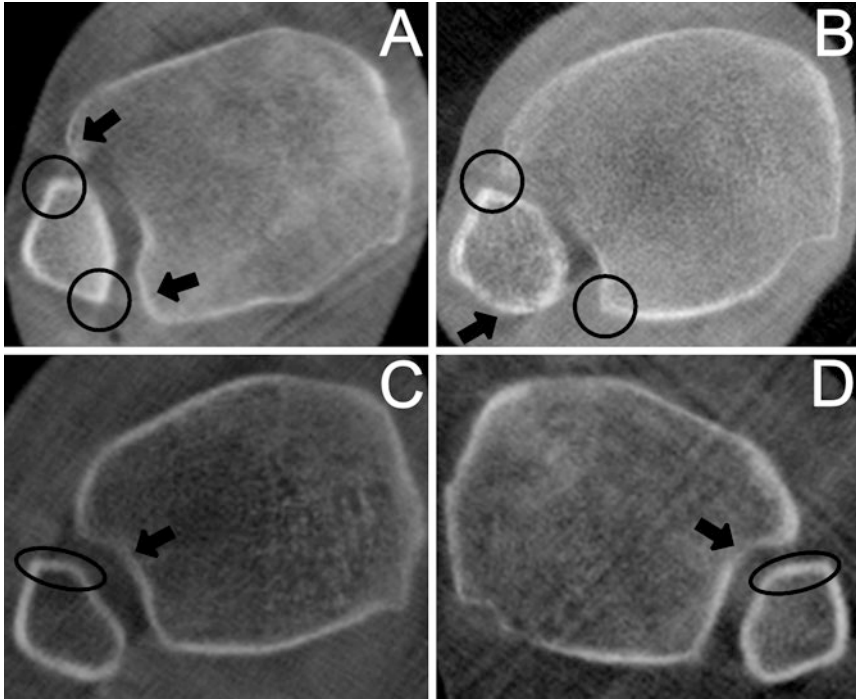*Significant difference (*P*-value <0.05)

Fig. 12.6 Axial CT images of three different cadavers 1 cm above of the medial edge of the distal tibial plafond. (**a**) Sharp edges are evident anterior and posterior of the fibula (circles), allowing accurate identification of the anteroposterior axis. The tibial incisura shows round anterior and posterior edges (arrows), making a reliable identification of the anterior and posterior margins difficult. (**b**) The anterior and posterior edges of the tibial incisura and the anterior edge of the fibula are well defined (circles), while the posterior edge of the fibula shows a rounded shape and is therefore difficult to identify (arrow). Such findings may negatively impact on the agreement of two-dimensional (2D) measurements on the level of the distal tibiofibular syndesmosis. (**c**) The native weight-bearing right ankle shows a different morphology on the level of the tibiofibular syndesmosis (anterior part of the fibula, circle; tibial incisura, arrow) compared to the (**d**) corresponding left side under the same conditions (anterior part of the fibula, circle; tibial incisura, arrow) [1]

A more experienced observer (e.g., fellowship-trained orthopedic surgeon) can perform 2D measurement on the level of the distal tibiofibular syndesmosis more accurately compared to a less experienced observer.

Our study has several limitations. First, the continuous loading and unloading for each experimental condition may provoke relaxation of soft tissues, impacting measurements. Second, freezing and thawing of tissue may further negatively impact the soft tissue condition. Also, some donors may have been inactive before time of death, which would negatively impact bone quality and, potentially, radiographic measurements. Third, resection of ligaments in cadavers can be done precisely. In a posttraumatic condition, different ligaments of the distal talo-fibular syndesmosis

are variably torn or ruptured. Over time, scar tissue may also form. Such complex injuries cannot be simulated accurately using cadaver models.

To conclude, load application does not impact on the ability of weight-bearing CT scans to diagnose incomplete and also more complete syndesmotic injuries in a cadaver model. Nevertheless, the ability to reliably position the foot during imaging is an advantage of weight-bearing CT technology over other imaging options.

References

1. Krähenbühl N, Bailey TL, Weinberg MW, Davidson NP, Hintermann B, Presson AP, Allen CM, Henninger HB, Saltzman CL, Barg A. Is load application necessary when using computed tomography scans to diagnose syndesmotic injuries? A cadaver study. Foot Ankle Surg. 2019. Feb 18, epub ahead of print.
2. Rammelt S, Obruba P. An update on the evaluation and treatment of syndesmotic injuries. Eur J Trauma Emerg Surg. 2015;41(6):601–14.
3. Krähenbühl N, Weinberg MW, Davidson NP, Mills MK, Hintermann B, Saltzman CL, Barg A. Imaging in syndesmotic injury: a systematic literature review. Skelet Radiol. 2018;47(5):631–48.
4. Hunt KJ, Goeb Y, Behn AW, Criswell B, Chou L. Ankle joint contact loads and displacement with progressive syndesmotic injury. Foot Ankle Int. 2015;36(9):1095–103.
5. LaMothe J, Baxter JR, Gilbert S, Murphy CI, Karnovsky SC, Drakos MC. Effect of complete syndesmotic disruption and deltoid injuries and different reduction methods on ankle joint contact mechanics. Foot Ankle Int. 2017;38(6):694–700.
6. Golano P, Vega J, de Leeuw PA, Malagelada F, Manzanares MC, Gotzens V, van Dijk CN. Anatomy of the ankle ligaments: a pictorial essay. Knee Surg Sports Traumatol Arthrosc. 2010;18(5):557–69.
7. Jeong MS, Choi YS, Kim YJ, Kim JS, Young KW, Jung YY. Deltoid ligament in acute ankle injury: MR imaging analysis. Skelet Radiol. 2014;43(5):655–63.
8. Feller R, Borenstein T, Fantry AJ, Kellum RB, Machan JT, Nickisch F, Blankenhorn B. Arthroscopic quantification of syndesmotic instability in a cadaveric model. Arthroscopy. 2017;33(2):436–44.
9. Schoennagel BP, Karul M, Avanesov M, Bannas P, Gold G, Grosterlinden LG, Rupprecht M, Adam G, Yamamura J. Isolated syndesmotic injury in acute ankle trauma: comparison of plain film radiography with 3T MRI. Eur J Radiol. 2014;83(10):1856–61.
10. Hermans JJ, Wentink N, Beumer A, Hop WC, Heijboer MP, Moonen AF, Ginai AZ. Correlation between radiological assessment of acute ankle fractures and syndesmotic injury on MRI. Skelet Radiol. 2012;41(7):787–801.
11. Krähenbühl N, Weinberg MW, Hintermann B, Haller JM, Saltzman CL, Barg A. Surgical outcome in chronic syndesmotic injury: a systematic literature review. Foot Ankle Surg. 2018. epub ahead of print.
12. Nielson JH, Gardner MJ, Peterson MG, Sallis JG, Potter HG, Helfet DL, Lorich DG. Radiographic measurements do not predict syndesmotic injury in ankle fractures: an MRI study. Clin Orthop Relat Res. 2005;436:216–21.
13. Barg A, Bailey T, Richter M, de Cesar Netto C, Lintz F, Burssens A, Phisitkul P, Hanrahan CJ, Saltzman CL. Weightbearing computed tomography of the foot and ankle: emerging technology topical review. Foot Ankle Int. 2018;39(3):376–86.
14. Lintz F, de Cesar Netto C, Barg A, Burssens A, Richter M, Weight Bearing CTISG. Weight-bearing cone beam CT scans in the foot and ankle. EFORT Open Rev. 2018;3(5):278–86.

15. Richter M, Seidl B, Zech S, Hahn S. PedCAT for 3D-imaging in standing position allows for more accurate bone position (angle) measurement than radiographs or CT. Foot Ankle Surg. 2014;20(3):201–7.
16. Shakoor D, Osgood GM, Brehler M, Zbijewski WB, de Cesar Netto C, Shafiq B, Orapin J, Thawait GK, Shon LC, Demehri S. Cone-beam CT measurements of distal tibio-fibular syndesmosis in asymptomatic uninjured ankles: does weight-bearing matter? Skelet Radiol. 2019;48(4):583–94.
17. Malhotra K, Welck M, Cullen N, Singh D, Goldberg AJ. The effects of weight bearing on the distal tibiofibular syndesmosis: a study comparing weight bearing-CT with conventional CT. Foot Ankle Surg. 2018. epub ahead of print.
18. Barg A, Amendola RL, Henninger HB, Kapron AL, Saltzman CL, Anderson AE. Influence of ankle position and radiographic projection angle on measurement of supramalleolar alignment on the anteroposterior and hindfoot alignment views. Foot Ankle Int. 2015;36(11):1352–61.
19. Nault ML, Hebert-Davies J, Laflamme GY, Leduc S. CT scan assessment of the syndesmosis: a new reproducible method. J Orthop Trauma. 2013;27(11):638–41.
20. Dikos GD, Heisler J, Choplin RH, Weber TG. Normal tibiofibular relationships at the syndesmosis on axial CT imaging. J Orthop Trauma. 2012;26(7):433–8.
21. Malhotra G, Cameron J, Toolan BC. Diagnosing chronic diastasis of the syndesmosis: a novel measurement using computed tomography. Foot Ankle Int. 2014;35(5):483–8.
22. Yeung TW, Chan CY, Chan WC, Yeung YN, Yuen MK. Can pre-operative axial CT imaging predict syndesmosis instability in patients sustaining ankle fractures? Seven years' experience in a tertiary trauma center. Skelet Radiol. 2015;44(6):823–9.
23. Nault ML, Marien M, Hebert-Davies J, Laflamme GY, Pelsser V, Rouleau DM, Gosselin-Papadopoulos N, Leduc S. MRI quantification of the impact of ankle position on syndesmosis anatomy. Foot Ankle Int. 2017;38(2):215–9.
24. Pneumaticos SG, Noble PC, Chatziioannou SN, Trevino SG. The effects of rotation on radiographic evaluation of the tibiofibular syndesmosis. Foot Ankle Int. 2002;23(2):107–11.
25. Mukhopadhyay S, Metcalfe A, Guha AR, Mohanty K, Hemmadi S, Lyons K, O'Doherty D. Malreduction of syndesmosis–are we considering the anatomical variation? Injury. 2011;42(10):1073–6.
26. Cherney SM, Spraggs-Hughes AG, McAndrew CM, Ricci WM, Gardner MJ. Incisura morphology as a risk factor for syndesmotic malreduction. Foot Ankle Int. 2016;37(7):748–54.
27. Lilyquist M, Shaw A, Latz K, Bogener J, Wentz B. Cadaveric analysis of the distal tibiofibular syndesmosis. Foot Ankle Int. 2016;37(8):882–90.
28. Elgafy H, Semaan HB, Blessinger B, Wassef A, Ebraheim NA. Computed tomography of normal distal tibiofibular syndesmosis. Skelet Radiol. 2010;39(6):559–64.
29. Burssens A, Vermue H, Barg A, Krahenbuhl N, Victor J, Buedts K. Templating of syndesmotic ankle lesions by use of 3D analysis in weightbearing and nonweightbearing CT. Foot Ankle Int. 2018;39(12):1487–96.